Halfvortices in Flat Nanomagnets

Gia-Wei Chern, David Clarke, Hyun Youk, and Oleg Tchernyshyov

Abstract We discuss a new type of topological defect in XY systems for which the $O(2)$ symmetry is broken in the presence of a boundary. Of particular interest is the appearance of such defects in nanomagnets with a planar geometry. They are manifested as kinks of magnetization along the edge and can be viewed as halfvortices with winding numbers $\pm 1/2$. We argue that the halfvortices play a role in flat nanomagnetics equally important to that of ordinary bulk vortices. We show that domain walls found in experiments and numerical simulations in strips and rings are composite objects containing two or more elementary defects. We also discuss a closely related system: the two-dimensional smectic liquid crystal films with planar boundary condition.

1 Introduction

It is well known that topological defects play an important role in catalyzing the transitions of physical systems with spontaneously broken symmetries [1, 2]. For instance, in nanorings made of soft ferromagnetic material, the switching process

G.-W. Chern
Department of Physics and Astronomy, The Johns Hopkins University, Baltimore, MD 21218, USA, e-mail: gwchern@pha.jhu.edu

D. Clarke
Department of Physics and Astronomy, The Johns Hopkins University, Baltimore, MD 21218, USA, e-mail: dclarke@pha.jhu.edu

H. Youk
Department of Physics, Massachusetts Institute of Technology, 77 Massachusetts Avenue, Cambridge, MD 02139, USA

O. Tchernyshyov
Department of Physics and Astronomy, The Johns Hopkins University, Baltimore, MD 21218, USA, e-mail: olegt@jhu.edu

B. Barbara et al. (eds.), *Quantum Magnetism.*

usually involves creation, propagation, and annihilation of domain walls with complex internal structure [3, 4]. We have pointed out in a series of papers [5, 6, 7] that domain walls in nanomagnets of planar geometry are composed of two or more elementary defects including ordinary vortices in the bulk and fractional vortices confined to the edge. As an example, the simplest domain wall in a magnetic strip consists of two edge defects with opposite winding numbers $n = \pm 1/2$.

In a nanomagnet with the geometry of a disk, the strong shape anisotropy (due to dipolar interaction) forces the magnetization vector $\mathbf{M}$ to lie in the disk plane, effectively making the magnet a 2D XY system. At the edge of the film, dipolar interaction further tries to align the spins to either of the two tangential directions of the edge: $\hat{\mathbf{m}} = \mathbf{M}/|\mathbf{M}| = (\cos\theta, \sin\theta) \pm \hat{\tau}$. The reduction of ground state symmetry from $O(2)$ to a discrete Z_2 allows for a new type of topological defect confined to the edge. These edge defects are manifested as kinks in magnetization $\hat{\mathbf{m}}$ along the boundary. In systems with discrete symmetry, such as the Ising ferromagnet, kinks are topological defects connecting different ground states. Their topological properties are rather simple [1]. Nevertheless, as two of us pointed out in Ref. [5], the edge defects can be viewed as halfvortices and have nontrivial topological charge related to the winding number of vortices in the bulk.

For a bounded flat nanomagnet, the winding number of vortices in the bulk is not a conserved quantity. This is illustrated by an example shown in Fig. 1, where a bulk vortex with winding number $n = +1$ is absorbed into the edge. Conservation of topological charges can be restored by assigning winding numbers to edge defects. In this case there are two such kinks at the edge of the film. The process shown in Fig. 1 then expresses the annihilation of an $+1$ bulk vortex with two $-\frac{1}{2}$ edge defects. Numerical simulations exhibiting similar annihilation of bulk vortex with edge defects can be found in Ref. [5].

The winding number of a single edge defect is defined as the line integral along the boundary $\partial\Omega$ [5]:

$$n = -\frac{1}{2\pi}\int_{\partial\Omega} \nabla(\theta - \theta_\tau)\cdot d\mathbf{r} = \pm\frac{1}{2}. \tag{1}$$

Examples of edge defects with winding numbers $\pm\frac{1}{2}$ are shown in Fig. 2. For a closed boundary the sum of the winding numbers of edge defects is also given by the above integral, but instead of integrating around one edge defect, the integral is carried out along the entire boundary. It was shown in Ref. [5] that this integral is related to the sum of winding numbers of vortices in the bulk. In general, for a film with g holes, we obtained

$$\sum_i^{\text{edge}} n_i + \sum_i^{\text{bulk}} n_i = 1 - g. \tag{2}$$

Here the winding numbers n_i are integers for bulk defects and half-integers for edge defects. This conservation law has important implications for the dynamics of

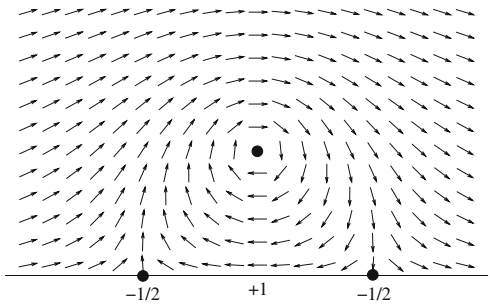

Fig. 1 A vortex ($n = +1$) absorbed by the edge can be viewed as its annihilation with two $-\frac{1}{2}$ edge defects. The annihilation results in a uniform magnetization pointing to the right

magnetization in nanomagnets [5]. As will be discussed in Section 3, defects with large winding numbers carry significant magnetic charge and thus are unfavored energetically in flat nanomagnets. Most of the intricate textures observed involve only bulk vortices with winding number $n = \pm 1$ and edge defects with $n = \pm\frac{1}{2}$.

Topological considerations also place important constraints on the possible structure of the domain walls in magnetic nanostrips [6]. Such domain walls play an important role in the switching dynamics of magnetic nanorings [16]. Examples of such domain walls are shown in Figs. 3 and 5. Since edge defects are kinks of magnetization along the boundary, a domain wall in a magnetic strip must contain an odd number of kinks at each edge. Furthermore, the angle of magnetization rotation along the two edges must be compensated by the winding number of the bulk. Consequently, the total topological charge including contributions of vortices and edge defects is zero.

The edge defects in nanomagnets are analogs of boojums at the surfaces and interfaces of superfluid ^{3}He [8, 9]. In general, "boojum" refers to a topological defect that can live only on the surface of an ordered medium [10]. Boojums were also predicted and observed in liquid crystals [11]. An interesting system which is closely related to our study of flat nanomagnets is the two-dimensional (2D) smectic C films. The vector nature of the order parameter $\hat{\mathbf{m}}$ is important to the confinement of halfvortices at the edge. For example it is well known that vortices with half-integer winding numbers are allowed to exist in the bulk of nematic liquid crystals. On the other hand, in 2D smectic C films, the in-plane ordering of molecular orientations is described by a 2D unit vector $\hat{\mathbf{c}}$ parallel to the smectic layers and pointing to the tilt direction [12]. Because rotating a tilted molecule by 180° around the normal of layers does not return it to its original configuration, this unit vector $\hat{\mathbf{c}}$, like the magnetization $\hat{\mathbf{m}}$, is a true vector. The system thus has edge-confined halfvortices similar to those in flat nanomagnets. We will discuss their structure in Section 4.

In this article we shall review the structure and energetics of halfvortices in nanomagnets. In contrast to the determination of the structure of topological defects in superfluids or liquid crystals where the energy is dominated by short range interactions, finding solutions of the vector field $\hat{\mathbf{m}}(\mathbf{r})$ for topological defects in

nanomagnets is considerably more difficult due to the nonlocal nature of dipolar interaction. We approached this problem from two opposite limits dominated by the exchange and dipolar interactions, respectively. The results are presented in Sections 2 and 3. Edge defects of smectic C films are discussed in Section 4, where we also point out the similarities and differences of the two models. We conclude with a summary of our major results in Section 5.

2 Exchange Limit of Flat Nanomagnets

The magnetic energy of a ferromagnetic nanoparticle has two major contributions: the exchange energy $A\int|\nabla\hat{\mathbf{m}}|^2\,d^3r$ and the dipolar energy $(\mu_0/2)\int|\mathbf{H}|^2\,d^3r$. The magnetic field $\mathbf{H}$ is related to the magnetization through Maxwell's equations, $\nabla\times\mathbf{H}=0$ and $\nabla\cdot(\mathbf{H}+\mathbf{M})=0$. Here we disregard the energy of anisotropy, which is negligible for soft ferromagnets such as permalloy.

Analytical treatment of topological defects is generally impossible due to the long range nature of dipolar interaction. One usually minimizes the energy numerically to find stable structures of the magnetization field. Nevertheless exact solutions are possible in a thin-film limit [13, 14]: $t\ll w\ll\lambda^2/t\ll w\log(w/t)$ defined for a strip of width w and thickness t. Here $\lambda=\sqrt{A/\mu_0M^2}$ is the length scale of exchange interaction. In this limit the magnetization only depends on the in-plane coordinates x and y, but not on z. Furthermore, the magnetic energy becomes a local functional of magnetization [13, 14]:

$$E[\hat{\mathbf{m}}(\mathbf{r})]/At=\int_\Omega|\nabla\hat{\mathbf{m}}|^2\,d^2r+(1/\Lambda)\int_{\partial\Omega}(\hat{\mathbf{m}}\cdot\hat{\mathbf{n}})^2\,dr. \tag{3}$$

Here Ω is the two-dimensional region of the film, $\partial\Omega$ is its line boundary, $\hat{\mathbf{n}}\perp\hat{\boldsymbol{\tau}}$ is unit vector pointing to the outward normal of the boundary, and $\Lambda=4\pi\lambda^2/t\log(w/t)$ is an effective magnetic length in the thin-film geometry. This is the familiar XY model [1] with anisotropy at the edge resulting from the dipolar interaction. Minimization of (3) with respect to θ yields the Laplace equation $\nabla^2\theta=0$ in the bulk and boundary condition $\hat{\mathbf{n}}\cdot\nabla\theta=\sin2(\theta+\theta_e)/\Lambda$ at the edge.

Topological defects that are stable in the bulk are ordinary vortices with integer winding numbers, which are well known in the XY model [1]. The boundary term of model (3) introduces yet another class of topological defects that have a singular core outside the edge of the system. To be explicit, consider an infinite semiplane $y>0$. Solutions satisfying the Laplace equation in the bulk and the boundary condition $\partial_y\theta=\sin2\theta/\Lambda$ at the edge $y=0$ are [5, 13]

$$\tan\theta(x,y)=\pm\frac{y+\Lambda}{x-X}. \tag{4}$$

The singular core is at $(X,-\Lambda)$, distance Λ outside of the edge. Figure 2 shows the magnetization fields of Eq. (4). As can be easily checked using Eq. (1) the winding

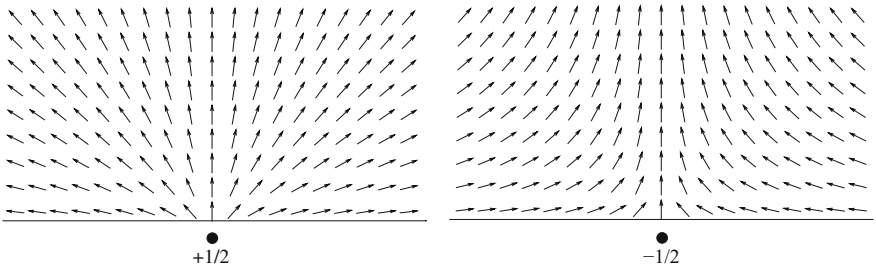

Fig. 2 Edge defects with winding numbers $n = +\frac{1}{2}$ (*left*) and $-\frac{1}{2}$ (*right*) in the exchange limit

numbers of these solutions are $\pm\frac{1}{2}$, respectively. The halfvortex cannot live in the bulk: as its singular core is moved inside the boundary, a string of misaligned spins occurs which extends from the core of halfvortex to the boundary [5]. The edge thus provides a linear confining potential for halfvortices.

In the limit $\Lambda/w \to 0$, magnetization at the edge is forced to be parallel to the boundary, $\hat{\mathbf{m}} = \pm\hat{\boldsymbol{\tau}}$. By exploiting the analogy between XY model and 2D electrostatics, one can use the method of images to deal with the effects introduced by the boundary [1, 5]. In this analogy the vortex is mapped to a point charge whose strength is given by the corresponding winding number. However, unlike in electrostatics, the "image" charge induced by the boundary has the same sign as the original. The above solution (4) with $\Lambda = 0$ looks just like a $n = \pm 1$ vortex with its core sitting at the edge. The assignment of half-integer winding number $n = \pm\frac{1}{2}$ to the edge defect is thus also consistent with the electrostatics analogy in the sense that the winding number is doubled by the reflection at the edge [5].

An exact solution for a domain wall was also obtained in this limit [5]. Consider a strip $|y| < w/2$. It has two ground states with uniform magnetization: $\theta = 0$ or π. Domain walls interpolating between the two ground states are given by

$$\tan\theta(x,y) = \pm\frac{\cos ky}{\sinh k(x-X)}, \tag{5}$$

where the wavenumber $k \approx \pi/(w+2\Lambda)$. The magnetization field of Eq. (5) (shown in Fig. 3) is reminiscent of 'transverse' domain walls (Bottom panel of Fig. 3) observed in micromagnetic simulations [15].

Unlike domain walls (kinks) in Ising magnet, a domain wall in a nanomagnet, e.g. Eq. (5), is a composite object containing two edge defects with opposite winding numbers $\pm\frac{1}{2}$. The singular cores of the two halfvortices reside outside the film, a distance Λ away from the edges. One can understand the stability of the domain wall using the electrostatics analogy: the attractive 'Coulomb' force pulling together the two halfvortices is balanced by the confining force from the edges.

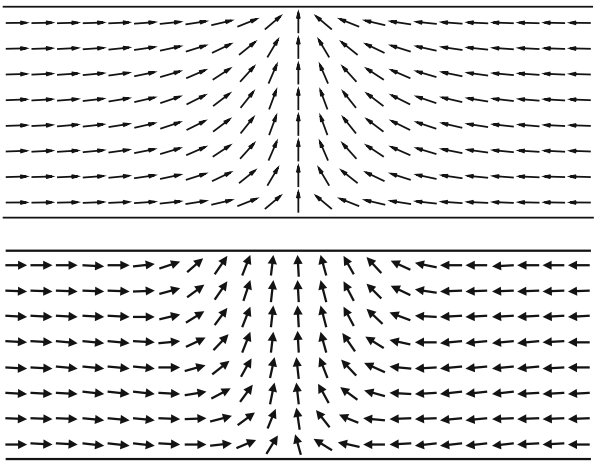

Fig. 3 *Top*: Magnetization of the head-to-head domain wall solution (5). It is composed of two edge defects with opposite winding numbers $\pm\frac{1}{2}$. *Bottom*: A transverse domain wall observed in a micromagnetic simulation using OOMMF [20] in a permalloy strip of width $w = 80\,\text{nm}$ and thickness $t = 20\,\text{nm}$

The total energy of the domain wall solution Eq. (5) evaluates to $E \approx 2\pi At(1 + \log(w/\pi\Lambda))$. As expected for the XY model, the exchange energy depends logarithmically on the system size, the width of the strip w in our case. It also depends logarithmically on a short distance cutoff which is provided by Λ here. After restoring the energy units and expressing Λ in terms of the relevant parameters, we obtain the following domain wall energy in the exchange limit

$$E_{\text{DW}} \approx 2\pi At \log\Big(\frac{ewt\log(w/t)}{\pi\lambda^2}\Big). \tag{6}$$

The energy depends linearly on the thickness of the film t and only weakly (logarithmically) on the width. These relations are important to the understanding of the hysteresis curves of asymmetric magnetic nanorings [16].

3 Dipolar Limit of Flat Nanomagnets

The thin-film limit discussed in the previous section is inaccessible to most experimental realizations of nanomagnets, in which the dipolar interaction is the primary driving force. In this section we discuss the structure and energetics of topological defects and domain walls in the opposite limit where the energy is dominated by the dipolar interaction. Our strategy here is first to find structures which minimize the magnetostatic energy $(\mu_0/2)\int|\mathbf{H}|^2 d^3r$ and then to include exchange interaction as a perturbation. However, energy minimization in the dipolar limit

is relatively difficult due to following reasons. Firstly, as opposed to the local exchange interaction, the dipolar interaction is long-ranged. Secondly, in many cases the magnetostatic energy has a large number of absolute minima. One thus has to search among these minima for one with the lowest exchange energy, making it a degenerate perturbation problem.

The magnetostatic energy of a given magnetization field $\hat{\mathbf{m}}(\mathbf{r})$ can also be expressed as the Coulomb interaction of magnetic charges with density $\rho_m(\mathbf{r}) = -M_0 \nabla \cdot \hat{\mathbf{m}}$, where M_0 is the saturation magnetization. Being positive definite, the magnetostatic energy has an absolute minimum of zero, which corresponds to a complete absence of magnetic charges. A general method to obtain the absolute minima of magnetostatic energy was provided by van den Berg in 1986 [17]. For magnetic films with arbitrary shapes, his method yields domains of slowly varying magnetization separated by discontinuous Néel walls. In the following we look for structures that have the desired winding number and are free of magnetic charges, i.e. $\nabla \cdot \hat{\mathbf{m}} = 0$ in the bulk and $\hat{\mathbf{n}} \cdot \hat{\mathbf{m}} = 0$ on the boundary.

We start by examining the vortex solutions of XY model. In polar coordinate, a vortex with winding number n is described by $\theta(x,y) = n\phi + \theta_0$, where θ_0 is a constant and $\phi = \arctan(y/x)$ is the azimuthal angle. Among these solutions, only the $n = 1$ vortex with $\theta_0 = \pi/2$ has zero charge density and survives in the dipolar limit. Its energy then comes entirely from the exchange interaction and diverges logrithmically with system size R: $E \approx 2\pi At \log(R/\lambda)$. Here the short distance cutoff is given by the exchange length λ.

The antivortex solutions of the XY model always carry a finite density of magnetic charge and thus are not a good starting point to obtain the $n = -1$ defect in the dipolar limit. Fortunately, a magnetization field with winding number -1 and free of bulk charges is realized by a configuration known as the cross tie (top panel of Fig. 4) [6, 18]. It consists of two 90° Néel walls normal to each other and intersecting at the singular core. The magnetization field of an antihalfvortex (winding

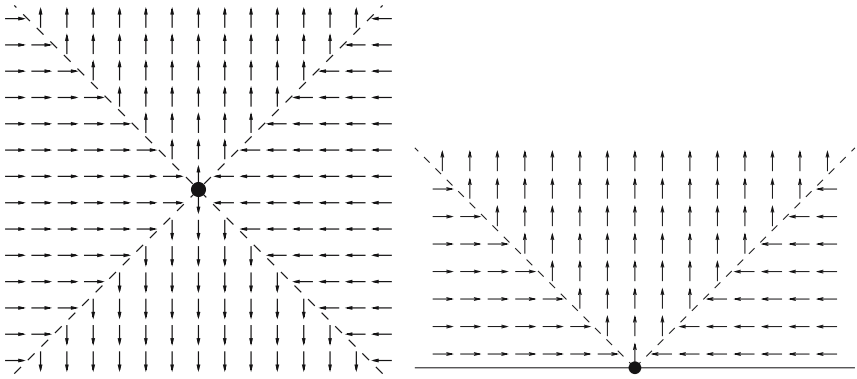

Fig. 4 An antivortex (*left*), and a $-\frac{1}{2}$ edge defect (*right*) in the dipolar limit

number $-\frac{1}{2}$) is obtained by placing the core of a cross tie at the edge of the film (bottom panel of Fig. 4). Since the magnetization along the edge is parallel to the boundary, the structure is also free of surface charge. As one moves from left to right along the edge the magnetization rotates counterclockwise through π. This is in agreement with the definition (1) for an antihalfvortex.

The energy of an antivortex or an antihalfvortex grows linearly with the length of the Néel walls L emanating from it:

$$E \sim \sigma t L + E_{\text{core}} \tag{7}$$

The surface tension of the wall σ has contributions from both exchange and dipolar interactions. In magnetic films with thickness exceeding the Néel-wall width (of order λ), it is given by [6]

$$\sigma = 2\sqrt{2}(\sin\theta_0 - \theta_0 \cos\theta_0) A/\lambda, \tag{8}$$

where $2\theta_0$ is the angle of magnetization rotation across the wall. In thinner films ($t \leq \lambda$) the magnetostatic term becomes substantially nonlocal and the Néel walls acquire long tails [19].

There is no charge-free configuration for the $+\frac{1}{2}$ edge defect. In addition, one could also observe from micromagnetic simulations that most of the magnetic charges of a transverse domain wall in a strip is accumulated around the $+\frac{1}{2}$ defect. Thus, in the dipolar limit, the magnetically charged $+\frac{1}{2}$ defect is prone to decay into a $-\frac{1}{2}$ edge defect and $+1$ vortex in the bulk. We next turn to the discussion of the structure of domain walls in this limit.

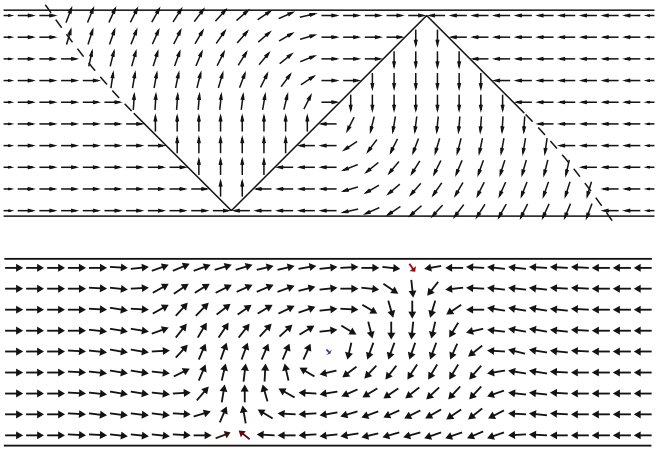

Fig. 5 *Top*: A magnetization configuration free of bulk magnetic charges, $-\nabla \cdot \mathbf{M} = 0$, and containing two $-1/2$ edge defects and a $+1$ vortex in the middle. Parabolic segments of Neel walls are shown by dashed lines. *Bottom*: A head-to-head vortex wall obtained in a micromagnetic simulation using OOMMF [20] in a permalloy strip of width $w = 500\,\text{nm}$ and thickness $t = 20\,\text{nm}$

An intrinsic problem arises when one tries to apply van den Berg's method to find the structure of domain walls. That is because a head-to-head domain wall carries a fixed nonzero amount of magnetic charge: $Q_m = 2M_0tw$. However, these magnetic charges tend to repel each other and spread over the surface of the sample, much the same as the electric charges in a metal. Based on this principle, we provided in Ref. [7] a construction of the head-to-head domain wall that is free of *bulk* magnetic charges. All of the charge Q_m is expelled to the edges. The resulting structure is shown in the top panel of Fig. 5. It resembles the structure known as the 'vortex' domain wall (bottom panel of Fig. 5) predicted to be stable in regimes dominated by dipolar interaction [15]. Both structures contain two $-\frac{1}{2}$ edge defects sharing one of their Néel walls and a $+1$ vortex residing at the midpoint of the common wall.

The variational construction contains charge-free domains with uniform and curling magnetization separated by straight and parabolic Néel walls. In a strip $|y| < w/2$, the two $-\frac{1}{2}$ edge defects share a Néel wall $x = y$ with the vortex core residing at (v, v) is located. The two curling domains in the regions $\pm v < \pm y < w/2$ are separated by parabolic Néel walls $(x - v)^2 = (2y \pm w)(2v \pm w)$ from domains with horizontal magnetization; they also merge seamlessly with other uniform domains along the lines $x = v$ and $y = v$.

The location (v, v) of the $+1$ vortex on the shared Néel wall is a free parameter of our variational construction. The structure remains free of bulk charge as the vortex core moves along the diagonal $x = y$. When it reaches one of the edge, its annihilation with the $-\frac{1}{2}$ edge defect creates a widely extended $+\frac{1}{2}$ edge defect. The resulting structure (top panel of Fig. 6) is topologically equivalent to the transverse domain wall (bottom panel of Figs. 3 and 6) discussed in the previous section.

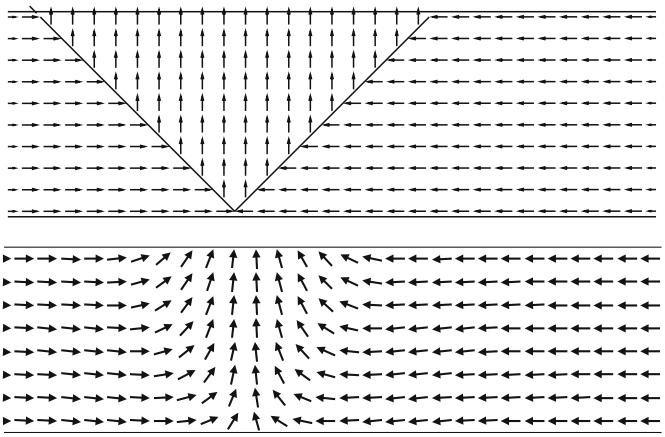

Fig. 6 *Top*: A model vortex wall when the vortex is absorbed by the edge forming an extended $+\frac{1}{2}$ edge defect along the upper boundary. *Bottom*: Transverse wall observed in micromagnetic simulation

The equilibrium structure for given strip width w and thickness t is determined by minimizing the total energy of the composite domain wall with respect to vortex coordinate v. The total energy contains the following terms. (a) The exchange energy of the two curling domains Ω around the vortex core. It is given by $At\int_{\Omega}(\nabla\theta)^2 d^2r$ and of the order $At\log(w/\lambda)$. (b) The energy of Néel walls, which can be computed as a line integral $t\int\sigma(\ell)\,d\ell$, where $d\ell$ is a line element of the wall. The surface tension σ, which depends on the angle of spin rotation across the wall, is given by Eq. (8). This term is of order Atw/λ. (c) The magnetostatic energy coming from the Coulomb interaction of magnetic charges spreading along the two edges. It is of the order $Aw(t^2/\lambda^2)\log(w/t)$.

By combining the above three contributions, the total energy curve $E(v)$ for a fixed width w and varying thickness t is shown in Fig. 7. For substantially wide and thick strips, the curve attains its absolute minimum as the vortex is in the middle of the strip, in agreement with numerical simulations [15]. A local minimum develops with the vortex core at the edge of the strip as the thickness decreases corresponding to the transverse wall shown in the bottom panel of Fig. 6. The transverse wall becomes the absolute minimum as the thickness is further reduced and the vortex wall ($v = 0$) is locally unstable. It should be noted that the above calculation for thin films, e.g. $t = 1$ nm, is only an extrapolation. For films with small cross section (but not in the exchange limit), our variational approach can not be trusted. Nonetheless, the method is illustrative and indeed shows that the three-defects wall structure is unstable when approaching the exchange limit.

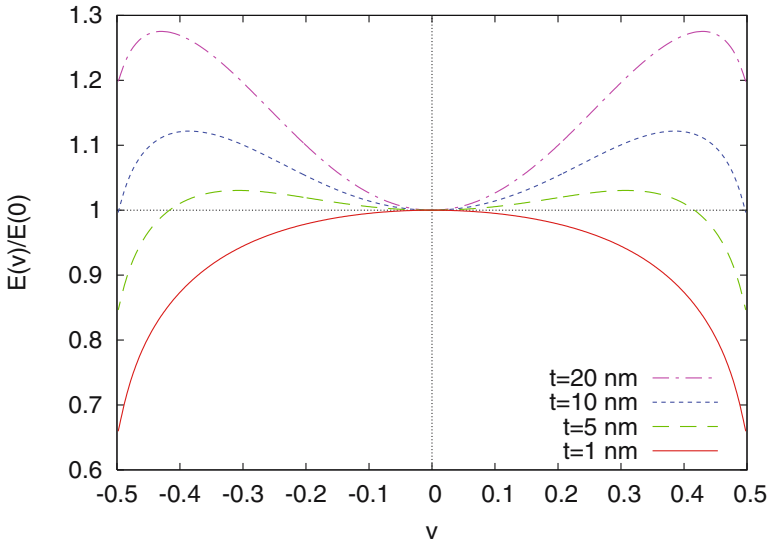

Fig. 7 Energy of the vortex domain wall as a function of the vortex position v at a fixed strip width $w = 50$ nm for several thicknesses t

4 Halfvortices in Smectic Films

The XY model discussed in the thin-film limit preserves a symmetry between topological defects with opposite winding numbers, namely, ± 1 vortices have exactly the same energy in model (3) (so do $\pm\frac{1}{2}$ edge defects). Since vortices of opposite winding numbers carry different magnetic charges, the degeneracy is lifted in thicker and wider strips where the dipolar interaction becomes more important. The configuration of the topological defects in the extreme dipolar limit discussed previously clearly shows this asymmetry. One can also break this symmetry by assigning different penalties to splay ($\nabla \cdot \hat{\mathbf{m}} \neq 0$) and bending ($\nabla \times \hat{\mathbf{m}} \neq 0$) deformations:

$$E[\hat{\mathbf{m}}(\mathbf{x})] = \int_{\Omega} [K_1(\nabla \cdot \hat{\mathbf{m}})^2 + K_2(\nabla \times \hat{\mathbf{m}})^2]\, d^2r + (1/\Lambda) \int_{\partial\Omega} (\hat{\mathbf{n}} \cdot \hat{\mathbf{m}})^2\, dr, \tag{9}$$

In the units where the energy is dimensionless, the elastic constants K_i are also dimensionless, whereas the edge anisotropy $1/\Lambda$ scales as the inverse length. With the unit vector $\hat{\mathbf{m}}$ identified with the $\hat{\mathbf{c}}$-director field, this energy functional describes the elastic energy of a chiral smectic film [21] or a Langmuir monolayer [22] with planar boundary conditions.

The case $K_1 = K_2$ corresponds to the XY model, which represents the exchange limit. By choosing $K_1 > K_2$ we discourage splay, which is similar to a penalty for magnetic charges in the bulk. The dipolar limit is similar to the regime where the bend energy is small compared to those of splay and edge anisotropy. In what follows we discuss the structure and energetics of topological defects in the extreme dipolar limit, $K_2 = 0$.

The $+1$ vortex solution $\theta(\mathbf{r}) = \phi + \pi/2$ remains an energy minimum of model (9) for arbitrary K_1 and K_2. The $+1/2$ edge defect in the XY limit, Eq. (4) with the '+' sign, also remains a stable configuration for arbitrary K_i and Λ except that the singular core is pushed further outside the boundary, a distance $(1+\varepsilon)\Lambda$ away from the edge. Here $\varepsilon = (K_1 - K_2)/(K_1 + K_2)$.

Since the bulk term of the energy functional (9) does not have an intrinsic length scale, an exact scale-invariant solution for an antivortex has been obtained in the 'dipolar' limit $K_2 = 0$:

$$\theta(x,y) = \phi - \arcsin(\sqrt{2}\sin\phi), \tag{10}$$

where $\phi = \arctan(y/x)$ is the azimuthal angle. The solution is singular at $\phi = \pm\pi/4$, where the first derivative $d\theta/d\phi$ diverges. A complete solution of the antivortex nevertheless can be obtained by continuing the above solution outside of the interval $|\phi| < \pi/4$ periodically. The result is shown in Fig. 8(a).

Analytical solutions for antihalfvortex for arbitrary Λ is yet to be found. In the limit $\Lambda \to 0$ achieved in boundaries with very strong anchoring force, the unit vector $\hat{\mathbf{m}}$ is forced to be parallel to the edge. In this limit, the $-\frac{1}{2}$ edge defect can be constructed following the same trick for antihalfvortex in the dipolar limit of nanomagnets. The resulting configuration is shown in Fig. 8(b). Compared with their

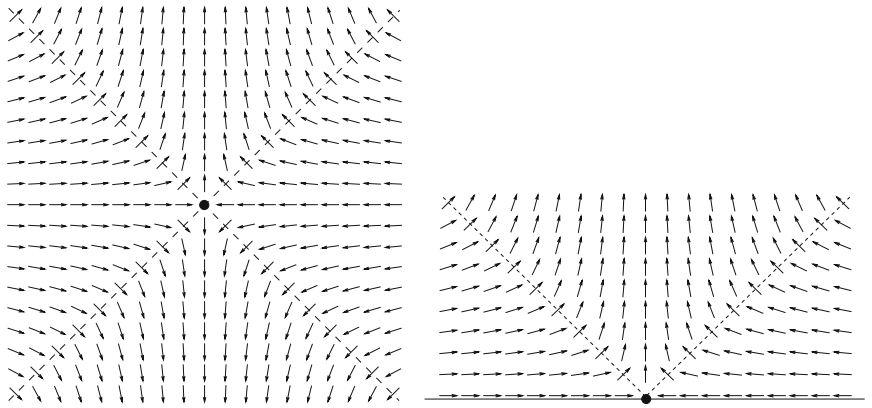

Fig. 8 An antivortex (**a**), and a $-\frac{1}{2}$ edge defect (**b**) in the elastic model with $K_1 = 1$, $K_2 = 0$, and $\Lambda = 0$

counterparts in the XY model, the antivortex and antihalfvortex in Fig. 8 are closer to the cross tie configuration (or half of it) shown in Fig. 4.

Although topological defects of the generalized elastic model show some similarities with those of the magnetic problem in the dipolar limit, there is an important difference regarding the scaling of their energy with system size. Since solution (10) is scale-invariant, the energy of the defects also diverges logrithmically with system size R: $E \sim \text{const} \times K_1 \log(R/a)$. Here a is a short distance cutoff. In the case of $-\frac{1}{2}$ edge defect, a is of the order of Λ. However, as discussed in the previous section, the energy of both antivortex and antihalfvortex scales linearly with the length of N eel wall. The nonlocal dipolar interaction in the magnetic problem results in a natural length scale $\lambda = \sqrt{A/\mu_0 M^2}$. By contrast, there is no such length scale in the elastic model (9), so the dependence of the energy on the system size is logarithmic.

5 Conclusion

We have discussed the topological properties of edge defects in XY systems with a broken $O(2)$ symmetry at the boundary. In particular, we discussed two physical systems containing such edge defects: the 2D smectic C films and nanomagnets with a planar geometry. Since spins at the boundary have two degenerate preferred directions (parallel or antiparallel to the boundary), the edge defects are manifested as kinks of magnetization along the edge. Moreover, they carry half-integer winding numbers and thus can be viewed as half-vortices confined at the edge. Conservation of the winding number can only be established by including contributions from the edge defects. As we have pointed out before [5, 6, 7], edge defects should be included along with ordinary vortices as the elementary topological defects in flat

nanomagnets. Indeed, domain walls in flat nanomagnets are composite objects consisting of two or more of the elementary defects. These walls play an important role in the dynamics of magnetization, especially in magnetic switching in strip or ring geometries.

We have also reviewed structures and energetics of the edge defects in two opposite limits dominated by the exchange and dipolar interactions, respectively. Analytical solutions of halfvortices and transverse domain walls were obtained in a thin-film limit where the exchange interaction is the dominant force determining the shape of topological defects. In this limit, the magnetic problem is reduced to the familiar XY model with an anisotropy at the edge. Domain walls stable in this regime are composed of two edge defects with winding number $\pm\frac{1}{2}$. By analogy with 2D electrostatics, the stability of transverse domain wall can be understood as resulting from a balance of the attractive Coulomb force between the oppositely charged halfvortices and the confining force from the edges.

Energy minimization is relatively difficult in the opposite limit dominated by the nonlocal dipolar interaction. Nevertheless, by treating the exchange interaction as a perturbation, we are able to find structures of topological defects stable in this regime. The $+1$ vortex of XY model with circulating magnetization remains a stable defect in the dipolar limit. The -1 vortex survives in this limit but is severely deformed; it has the cross tie structure consisting of two 90° Néel walls intersecting at the singular core. The configuration of the $-\frac{1}{2}$ edge defect is constructed by placing the core of a cross tie at the boundary. The $+\frac{1}{2}$ defect carries a finite amount of magnetic charge and is unstable in this limit.

A vortex domain wall composed of two $-\frac{1}{2}$ edge defects and a $+1$ vortex in the bulk is stable in the dipolar limit. We have presented a variational construction of the vortex domain wall which is free of bulk magnetic charge. By varying the location of the center $+1$ vortex, the construction interpolates between the vortex wall and the transverse wall. Variational calculation of the domain wall energy reveals that the vortex wall is indeed stable in the dipolar limit whereas it becomes an energy maximum in thin and narrow strips.

Finally, we have discussed structures of topological defects in an elastic model which generalizes the XY model of the thin-film limit. Calculations in this model are simplified by the replacement of non-local interactions between magnetic charges by a term that penalizes the existence of magnetic charge in a local fashion. This model is strictly applicable to smectic C films, but may provide insight into magnetic configurations. In particular, the allowed topological defects are the same in both systems, due to the identical group structure of the two models both in the bulk and on the boundary.

Acknowledgements We thank C.-L. Chien, P. Fendley, D. Huse. R. L. Leheny, P. Mellado, O. Tretiakov, and F. Q. Zhu for helpful discussions. The work was supported in part by the NSF Grant No. DMR05-20491.

References

1. Chaikin, P.M., Lubensky, T.C.: *Principles of Condensed Matter Physics*, Cambridge University Press, Cambridge, (2000).
2. Mermin, N.D.: Rev. Mod. Phys. **51**, 591 (1979).
3. Zhu, J.-G., Zheng, Y., Prinz, G. A.: J. Appl. Phys. **87**, 6668 (2000).
4. Kläui, M., Vaz, C.A.F., Lopez-Diaz, L., Bland, J.A.C.: J. Phys.: Condens. Matter **15**, R985 (2003).
5. Tchernyshyov, O., Chern, G.-W.: Phys. Rev. Lett. **95**, 197204 (2005).
6. Chern, G.-W., Youk, H., Tchernyshyov, O.: J. Appl. Phys. **99**, 08Q505 (2006).
7. Youk, H., Chern, G.-W., Merit, K., Oppenheimer, B., Tchernyshyov, O.: J. Appl. Phys. **99**, 08B101 (2006).
8. Mermin, N.D.: pp. 3–22 In: *Quantum Fluids and Solids*, eds. S.B. Trickey, E.D. Adams and J.W. Dufty, Plenum, New York (1977).
9. Misirpashaev, T.Sh.: Sov. Phys. JETP **72**, 973 (1991).
10. Volovik, G.E.: *The Universe in a Helium Droplet*, Clarendon Press, Oxford (2003).
11. Kleman, M., Lavrentovich, O.D.: *Soft Matter Physics*, Springer, New York (2003).
12. deGennes, P.G., Prost, J.: *The Physics of Liquid Crystals*, Clarendon Press, Oxford (1993).
13. Kurzke, M.: Calc. Var. PDE **26**, 1 (2006).
14. Kohn, R.V., Slastikov, V.V.: Proc. Roy. Soc. (London) Ser. A **461**, 143 (2005).
15. McMichael, R.D., Donahue, M.J.: IEEE Trans. Magn. **33**, 4167 (1997).
16. Zhu, F.Q., Chern, G.-W., Tchernyshyov, O., Zhu, X.C., Zhu, J.G., Chien, C.L.: Phys. Rev. Lett. **96**, 027205 (2006).
17. van den Berg, H.A.M.: J. Appl. Phys. **60**, 1104 (1986).
18. Londorf, M., Wadas, A., van den Berg, H.A.M., Wiesendanger, R.: Appl. Phys. Lett. **68**, 3635 (1996).
19. Hubert, A., Schaefer, R.: *Magnetic Domains*, Springer, Berlin (1998).
20. Donahue, M.J., Porter, D.G.: OOMMF User's Guide, Version 1.0, In: Interagency Report NISTIR 6376, NIST, Gaithersburg (1999). http://math.nist.gov/oommf/
21. Langer, S.A., Sethna, J.P.: Phys. Rev. A **34**, 5035 (1986).
22. Fischer, T.M., Bruinsma, R.F., Knobler, C.M.: Phys. Rev. E **50**, 413 (1994).